Int. J. Electrochem. Sci., 10 **(2015)** 5382 - 5394

International Journal of
ELECTROCHEMICAL
SCIENCE
www.electrochemsci.org

Properties of Stannum-Based Li-NASICON-Structured Solid Electrolytes for Potential Application in Electrochemical Devices

N. A. Mustaffa[1,2,*], *N. S. Mohamed*[3,*]

[1]Institute of Graduate Studies, University of Malaya, 50603 Kuala Lumpur, Malaysia.
[2]Faculty of Applied Sciences, Universiti Teknologi MARA, 40450 Selangor, Malaysia.
[3]Centre for Foundation Studies in Science, University of Malaya, 50603 Kuala Lumpur, Malaysia.
[*]E-mail: nuramalina@salam.uitm.edu.my; nsabirin@um.edu.my

Received: 23 April 2015 / *Accepted:* 16 May 2015 / *Published:* 27 May 2015

The aim of this study was to synthesize NASICON-structured $LiSn_2P_3O_{12}$ solid electrolytes by the citric acid assisted sol-gel method upon sintering for 48 hours instead of 24 hours, as reported in our previous study. X-ray diffraction analysis confirmed the formation of a rhombohedral phase of a NASICON-type structure upon sintering at 600 and 650 °C for 48 hours. By sintering a sample of $LiSn_2P_3O_{12}$ at a temperature of 600 °C, a conductivity of 1.38 $\times 10^{-5}$ Scm^{-1} at 500 °C was obtained. Meanwhile, a lower conductivity of 1.03 x 10^{-5} Scm^{-1} at 500 ^{o}C was obtained when the $LiSn_2P_3O_{12}$ sample was sintered at a temperature of 650 °C. The decomposition voltage reached 4.8 V for the highest conducting $LiSn_2P_3O_{12}$ sample sintered at 600 °C. Thus, the current results show that $LiSn_2P_3O_{12}$ is a promising candidate for applications as a solid electrolyte in elevated temperature electrochemical devices.

Keywords: Stannum; NASICON-structured; Solid electrolyte; Ionic conductivity

1. INTRODUCTION

Increasing demands for high-energy power sources have led to the development of power sources technology. Due to their high ionic conductivity, solid electrolytes have proven to be viable for use in power sources industries, and are generally used as components in innovative electrochemical appliances such as batteries, fuel cells, gas separation membranes, chemical sensors and ionic switches [1]. On the other hand, compared to solid electrolytes, liquid electrolytes that are used commercially possess a number of disadvantages, some of which are that they only function within a limited range of temperatures; the electrolyte solution may corrode the electrode and cause the device to malfunction;

and they are subject to leakage [2]. In view of these shortcomings, a suitable and ideal solid electrolyte would be one that possesses a high ionic conductivity (< 10^{-4} S cm^{-1}) at a wide range of operating temperatures, a low electronic conductivity, as well as good electrochemical stability window with regard to electrodes (> 4.5 V). Moreover, solid electrolytes come in simple designs, can provide a natural seal, are able to withstand shocks and vibrations, as well as changes in pressure and temperature, have greater electrochemical stability, and are much safer [3].

Among the many solid electrolytes available, NASICON (Sodium Super Ionic Conductor) has been extensively tested for use in power sources. NASICON is better than other electrolyte materials in terms of its high ionic conductivity, its stable phosphate units and its high melting point (> 1650 °C) [5]. It was first discovered by Goodenough et al. (1976) and its general formula is $Na_{1+x}Zr_2Si_xP_3O_{12}$. The NASICON compound basically has a rhombohedral ($R\bar{3}c$) symmetrical structure comprised of a three-dimensional framework, with the corners being made up of ZrO_6 octahedra and PO_4 tetrahedra. In all NASICON compounds, the Li^+ ion conductor, $LiSn_2P_3O_{12}$ has been the least studied compared to $LiTi_2P_3O_{12}$ [6-10]. The main challenge with regard to this compound is to increase its ionic conductivity, as previous researchers have reported that it has a low ionic conductivity of between ~10^{-7} S cm^{-1} and ~10^{-10} S cm^{-1} [8; 11 – 15]. Alternatively, a simple and economical sol-gel method may be used to prepare $LiSn_2P_3O_{12}$ NASICON-structured materials as this method can result in a lower synthesis temperature that is favourable for obtaining a higher ionic conductivity in highly homogeneous materials [16 - 17]. In previous work, NASICON rhombohedral-structured $LiSn_2P_3O_{12}$ solid electrolytes were successfully obtained via the citric acid assisted sol-gel method upon sintering at 600 °C for 24 hours with minor traces of SnP_2O_7 impurity [18]. The conductivity of the prepared sample at 500 °C was 1.40 x 10^{-5} S cm^{-1}, which is one order of magnitude higher than that reported in an earlier work by Norhaniza et al. (2010), and four orders of magnitude higher than that reported by Martinez-Juarez et al. (1997) and Lazarraga et al. (2004).

In the present study, $LiSn_2P_3O_{12}$ samples were synthesized by means of the citric acid assisted sol-gel method, but the sintering process was carried out for a longer period of time, that is 48 hours. The longer sintering time was expected to lead to the decomposition of the minor traces of SnP_2O_7 impurity that was found in the previous study. On the other hand, the sintering temperatures of 600 and 650 °C were chosen based on the thermal test in the previous study. Next, X-ray diffraction (XRD), Fourier transform infrared (FTIR), scanning electron microscopy (SEM), particle size analysis, energy dispersive X-ray (EDX), impedance spectroscopy (IS), linear sweep voltammetry (LSV) and transference number measurements were employed to examine the structural, thermal, electrical and electrochemical properties of the $LiSn_2P_3O_{12}$ samples .

2. EXPERIMENTAL PROCEDURES

2.1 Synthesis of $LiSn_2P_3O_{12}$ Samples

The $LiSn_2P_3O_{12}$ samples were prepared by means of the citric acid assisted sol-gel method. All the chemicals were of analytical grade and were directly used as received without further purification. The starting materials used were lithium acetate (CH_3COOLi), stannum (IV) chloride pentahydrate ($SnCl_4.5H_2O$) and ammonium phosphate ($H_{12}N_3O_4P$), while the chelating agent was citric acid,

($C_6H_80_7$) and the solvent was distilled water. Firstly, CH_3COOLi, $SnCl_4.5H_2O$ and $H_{12}N_3O_4P$ in the molar ratio of 1:2:3 were dissolved in distilled water under magnetic stirring. Citric acid ($C_6H_8O_7$), polyethylene glycol ($C_2H_6O_2$) and ammonium hydroxide (NH_4OH) were then mixed together into the previously prepared solution under magnetic stirring. $C_2H_6O_6$ and NH_4OH were added to promote polyesterification and polycondensation. The molar ratio of $C_2H_6O_6$:NH_4OH was 1:1. Next, the solution was shifted into a reflux system and was stirred constantly for 24 hours to form a homogenous solution. The solution was then removed and vaporized under magnetic stirring for approximately 4 hours at a temperature of 80 °C. Then, the gel that was produced was dried in an oven for 24 hours at 150 °C so as to get rid of water particles, resistant organic groups and also to prevent ceramic cracks. The resulting precursor powder was then ground finely for 30 minutes before being subjected to an annealing process at two different temperatures of 600 and 650 °C for 48 hours. The final product was then ground again for another 30 minutes before a Specac hydraulic press under a pressure of 5 tons was used to form the powder into pellets with a 13 mm-diameter and thickness of between 1.00 – 2.00 mm.

2.2 Characterization techniques

The samples were subjected to structural analysis by means of XRD using a PaNalytical – X'pert^3 x-ray diffractometer with Cu-K_α radiation of wavelength of 1.5406 Å. The 2θ ranged from 10 ° to 45 ° and was 0.026 ° with regard to step size. A Zeiss-Evo MA10 scanning electron microscope was used to conduct a morphological analysis of the $LiSn_2P_3O_{12}$ powders, while energy dispersive X-ray using an Oxford Aztec X-Act EDX spectrometer attached to the scanning electron microscope was used to perform an elemental analysis of the powders. A FRITSCH Laser Particle Sizer Analysette 22 NanoTec was used to derive information on the particle size of the electrolytes at room temperature. The impedance of the sintered pellets was measured by AC impedance spectroscopy using a Solatron 1260 impedance analyser over a frequency range of between 1 to 10 MHz. The applied voltage was set at 200 mV and all the measurements were taken at temperatures of between 30 to 500 °C. The electrochemical stability window of the electrolytes system was investigated by using the Wonatech ZIVE MP2 multichannel electrochemical workstation. LSV measurement was conducted at room temperature at a scan rate of 5 mV s^{-1}. Wagner's D.C. polarization method was employed to assess the ionic transference number measurement. The sample was inserted between two stainless steel blocking electrodes and a potential current of 0.5 V was applied in order to polarize it. The current was then monitored as a function of time until it reached a steady state condition.

3. RESULTS AND DISCUSSIONS

3.1 X-ray Diffraction Analysis

The X-ray diffraction patterns of the $LiSn_2P_3O_{12}$ samples sintered at (a) 600 ^oC and (b) 650 °C are shown in Figure 1. A rhombohedral NASICON-type symmetrical structure ($R\bar{3}c$) was successfully obtained upon sintering at 600 and 650 °C for 48 hours in the presence of unreacted SnO_2 [9]compared

to the sintering of the $LiSn_2P_3O_{12}$ samples for 24 hours, whereby there still remained slight traces of SnP_2O_7 impurity peaks [18], thus implying that SnP_2O_7 takes a longer time to decompose.

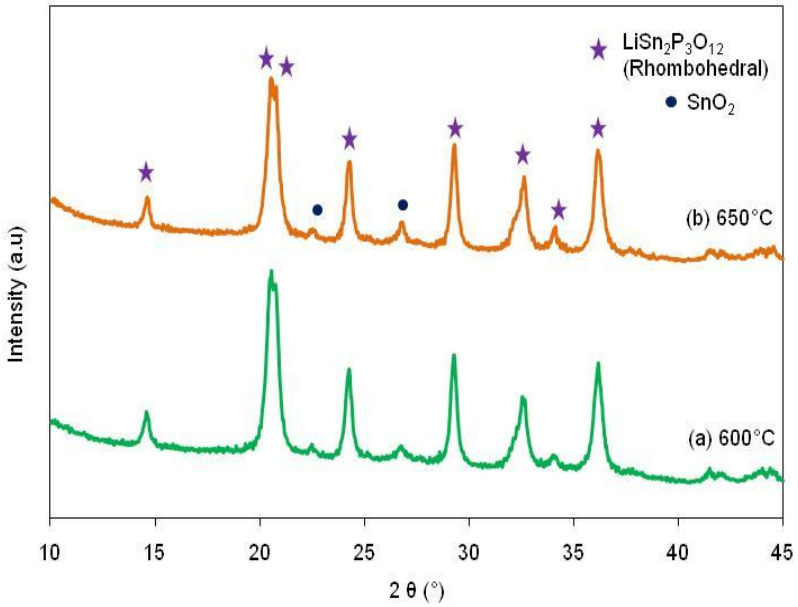

Figure 1. X-ray diffractograms $LiSn_2P_3O_{12}$ samples sintered at (a) 600 and (b) 650 °C upon sintering for 48 hours.

All the peaks observed in the $LiSn_2P_3O_{12}$ XRD pattern matched those reported in our previous work, thus, clearly indicating that the sol-gel method can be used to produce less impurity compound compared to other methods, such as the mechanical milling method that was used by Norhaniza et al. (2010). Besides that, unlike our earlier work where the double, rhombohedral and triclinic phases were found to coexist in the $LiSn_2P_3O_{12}$ samples sintered at 650 ^oC, in the current work only one phase, namely the rhombohedral phase, was detected in the samples sintered at the same temperature [18]. The following formula was then used to calculate the lattice parameters of the samples:

$$\frac{1}{d^2} = \frac{4}{3}\left(\frac{h^2+hk+k^2}{a^2}\right) + \frac{l^2}{c^2} \quad (1)$$

The crystallite size was determined by applying Scherrer's equation as given below:

$$D = \frac{k\lambda}{\beta cos\theta} \quad (2)$$

where *k* denotes a Scherer constant value (0.94), λ denotes the wavelength of the source (1.5406 Å), β denotes the FWHM (in radians), and θ denotes the Bragg angle (in radians).

Table 1. Lattice parameters, unit cell volume and density of $LiSn_2P_3O_{12}$ samples sintered at 600 and 650 °C

Sintering Temperature (°C)	*a* [Å]	*c* [Å]	*V* [Å^3]	Crystallite size [Å]	Density [g cm^{-3}]
600	8.3880	22.0148	1341.38	137.4	3.51
650	8.4071	21.9985	1346.50	138.3	3.49

The lattice parameters, unit cell volume and density of both the sintered electrolyte samples are presented in Table 1. From the table, it can be seen that the values of *a*, *c* and *V* for the $LiSn_2P_3O_{12}$ samples sintered at 600 °C were 8.3880 Å, 22.0148 Å and 1341.38 Å^3, respectively, while for the samples sintered at 650 °C, these values were 8.4071 Å, 21.9985 Å and 1346.50 Å^3, respectively. At the same time, an increase in the sintering temperature from 600 to 650 ^{o}C was accompanied by an increase in the crystallite size, as evidenced by the narrowing of the peak, which indicates bigger grains [19]. Meanwhile, the densities of both the sintered electrolyte samples were more than 90 % of its theoretical density of 3.79 g cm^{-3}, with the highest density being that of the $LiSn_2P_3O_{12}$ samples sintered at 600 °C, which is attributed to the compactness of the tiniest crystallites in the system [1] in accordance with the same pattern in our earlier work.

3.2 Scanning electron microscopy, energy dispersive X-ray spectroscopy and particle size distribution analysis

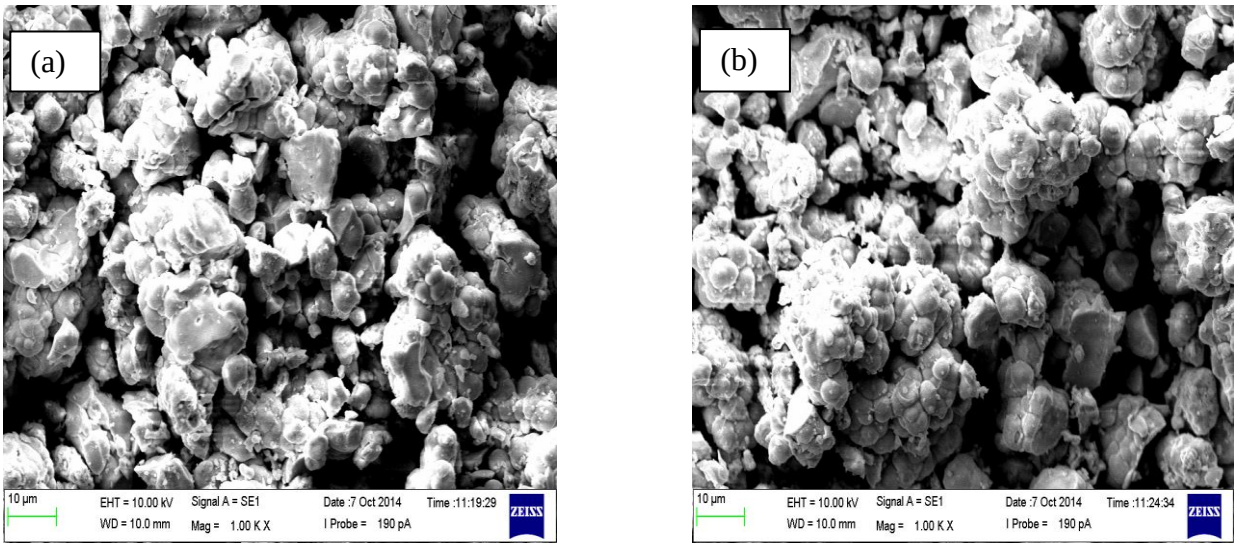

Figure 2. SEM micrographs of $LiSn_2P_3O_{12}$ samples sintered at (a) 600 and (b) 650 °C.

The SEM micrographs of the $LiSn_2P_3O_{12}$ samples sintered at 600 and 650 °C are shown in Figure 2. From the SEM micrographs it can be seen that the powders in both samples are slightly agglomerated. Meanwhile, EDX spectroscopy was performed on both the $LiSn_2P_3O_{12}$ samples to

analyse their elements. The results of the EDX analysis of the samples sintered at 600 and 650 °C are presented in Table 2.

Table 2. EDX stoichiometric atomic ratios for $LiSn_2P_3O_{12}$ samples sintered at 600 and 650 °C

Sintering Temperature (°C)	Composition	Stoichiometric atomic ratio		
		Sn	P	O
	Starting mixture	2	3	12
600	EDX analysis	2.00	2.63	12.60
650	EDX analysis	2.00	2.68	12.60

Only the presence of Sn, P and O appear in the EDX spectra, while the light atomic weight of lithium prevents its emitted radiation from being detected by EDX. As such, the general idea of charge neutrality can be applied for this case [13], whereby the EDX ratios of the elements in all the samples correspond with the stoichiometric ratios of the starting materials.

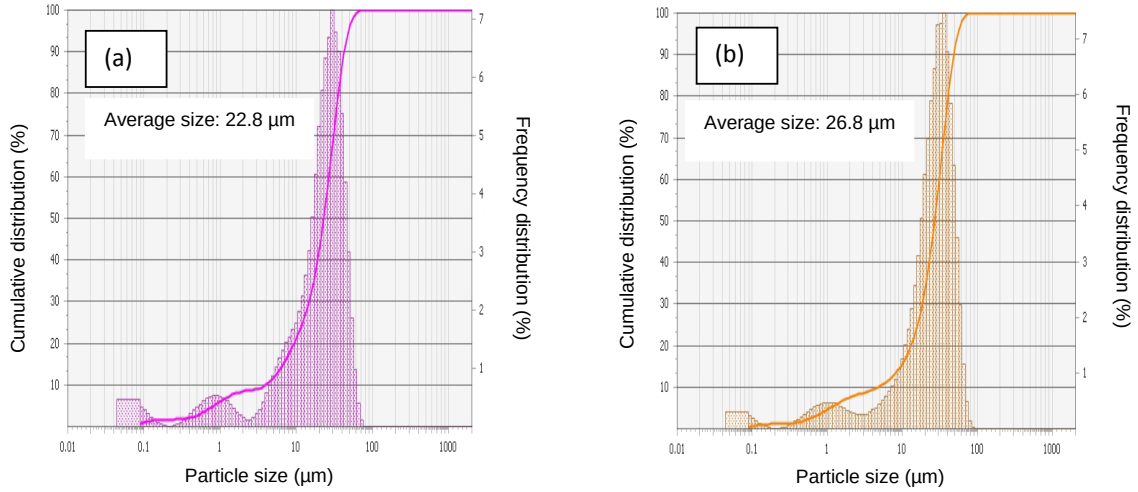

Figure 3. Particle size distributions of $LiSn_2P_3O_{12}$ samples sintered at (a) 600 and (b) 650 °C.

The particle size distributions of the $LiSn_2P_3O_{12}$ samples sintered at (a) 600 and (b) 650 °C are shown in Figure 3. From the graphs it can be clearly seen that the size of the particles in $LiSn_2P_3O_{12}$ samples increased together with the sintering temperature. As the sintering temperature was raised from 600 °C to 650 °C, the average size of the particles in the $LiSn_2P_3O_{12}$ samples grew from 22.8 µm to 26.8 µm. On correlating these results with the X-ray diffraction analysis, it was found that as the sintering temperature increased, so did the crystallite size of the prepared samples. The size of the particles in both the sintered samples was also slightly higher than that of $LiSn_2P_3O_{12}$ samples sintered for 24 hours in our previous work [18].

3.4 Impedance Analysis

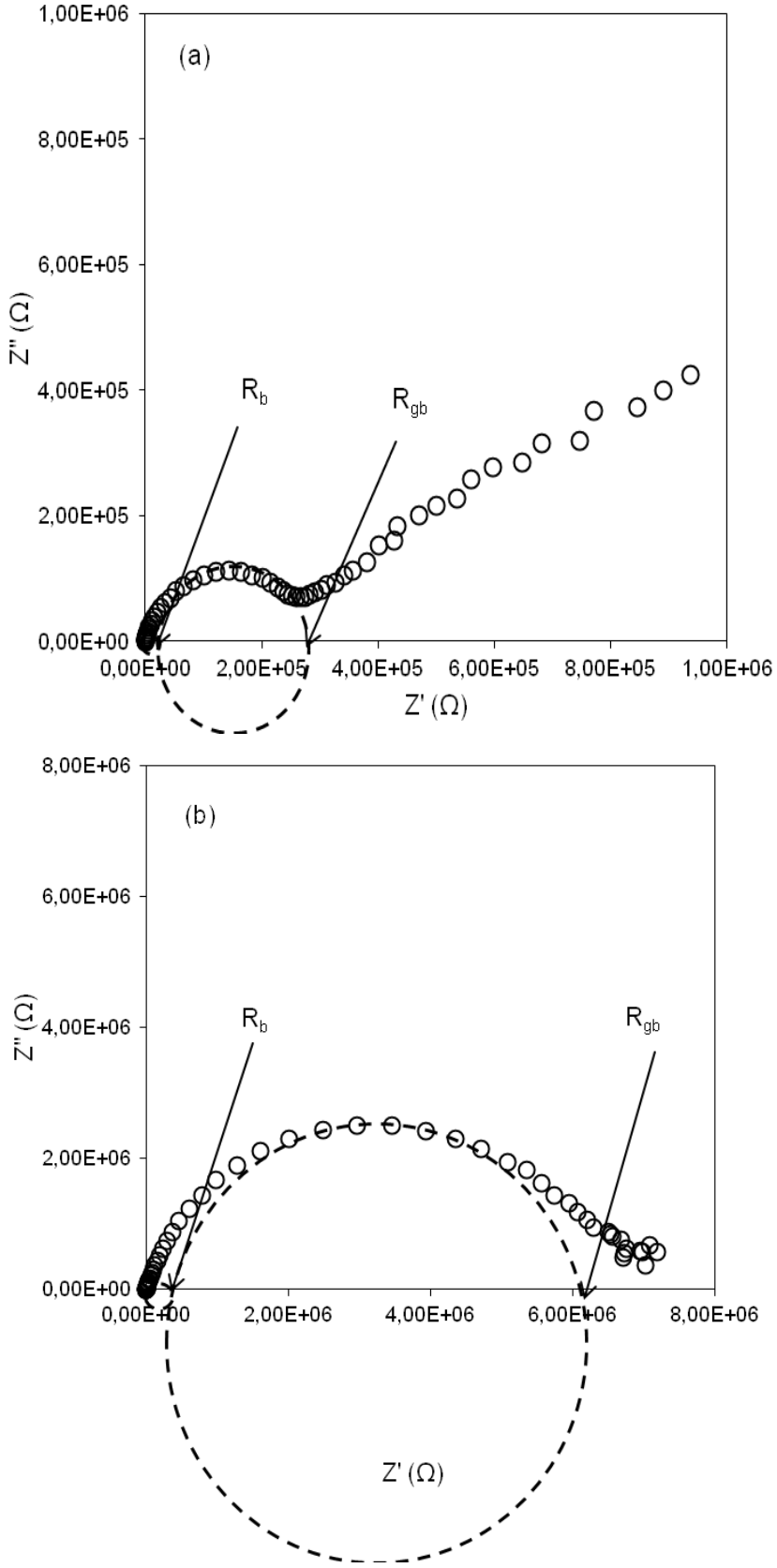

Figure 4. Cole-Cole plot of $LiSn_2P_3O_{12}$ sample at 30 °C sintered at (a) 600 and (b) 650 °C.

The Cole-Cole plots of the $LiSn_2P_3O_{12}$ sample at 30 °C are depicted in Fig. 4, with Fig. 4(a) and Fig. 4(b) representing the plots of the samples sintered at 600 °C and at 650 °C, respectively. Just like the pattern in our earlier work, both plots are comprised of two semicircles that overlap each other, with the region of low frequency being denoted by a spike [18]. The bulk response is represented by the high frequency semicircle, while its intersection with the X-axis represents the bulk resistance, R_b. Meanwhile, the grain boundary response is represented by the middle frequency semicircle, with its intersection with the X-axis being the grain boundary resistance, R_{gb} [13]. The spike that can be clearly seen at the low frequency region of the $LiSn_2P_3O_{12}$ sample sintered at 600 °C may indicate the effects of electrode polarization as a result of the accumulation of ions between the electrode and the sample [20].

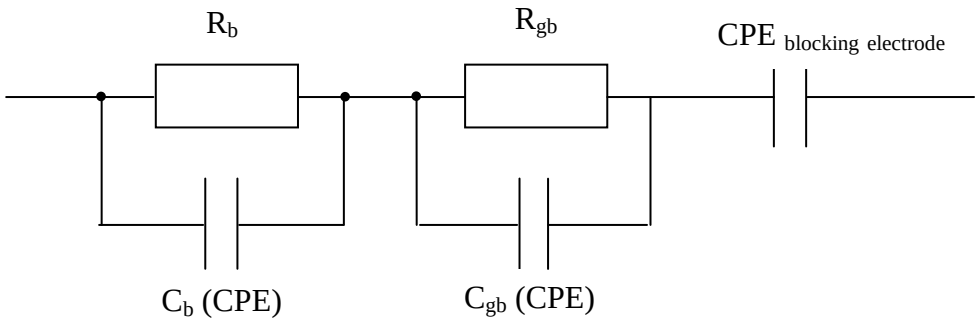

Figure 5. Equivalent circuit of $LiSn_2P_3O_{12}$ samples based on the impedance analysis of the samples at room temperature.

In addition, Figure 5 shows that the complex impedance data obtained experimentally for the $LiSn_2P_3O_{12}$ samples at room temperature may be approximately denoted by the impedance of an equivalent circuit comprised of bulk and grain boundary resistance R_b and R_{gb}, respectively, and the bulk and grain boundary capacitance C_b (CPE) and C_{gb} (CPE), respectively, and the $CPE_{blocking\ electrode}$ with a constant phase element (CPE) behaviour [21]. The general expression of the CPE is [22-23]

$$Z_{CPE} = \frac{1}{C\,(j\omega)^n} \quad (3)$$

where C is the ideal capacitance when $n = 1$, $j = (-1)^{1/2}$ and ω is the angular frequency, where $\omega = 2\pi f$.

Table 3. Ionic conductivity at 30 and 500 °C for $LiSn_2P_3O_{12}$ samples sintered at 600 and 650 °C

Sintering Temperature (°C)	$\sigma_{b,500}$ (S cm^{-1})	$\sigma_{b,30}$ (S cm^{-1})	$\sigma_{gb,30}$ (S cm^{-1})	$\sigma_{t,500}$ (S cm^{-1})	$\sigma_{t,30}$ (S cm^{-1})
600	1.38×10^{-5}	7.22×10^{-6}	2.99×10^{-7}	1.38×10^{-5}	2.87×10^{-7}
650	1.03×10^{-5}	3.28×10^{-6}	1.79×10^{-8}	1.03×10^{-5}	1.78×10^{-8}
600 [18]	1.40×10^{-5}	1.05×10^{-6}	4.24×10^{-8}	1.40×10^{-5}	4.08×10^{-8}
650 [18]	3.64×10^{-5}	1.15×10^{-6}	5.79×10^{-8}	3.64×10^{-5}	5.51×10^{-8}

The bulk and grain boundary conductivities, σ_b and σ_{gb}, respectively can then be computed from the Cole-Cole plot by means of the following equations:

$$\sigma_b = \frac{d}{AR_b} \quad \text{and} \quad \sigma_{gb} = \frac{d}{AR_{gb}} \tag{4}$$

where d is the thickness of the sample, A is the area of the cross-section of the sample, R_b is the bulk resistance and R_{gb} is the grain boundary resistance. Table 3 compares the values of both σ_b and σ_{gb} at 30 and 500 °C for the $LiSn_2P_3O_{12}$ samples sintered at 600 and 650 °C with the values obtained for the samples in the earlier study. For the $LiSn_2P_3O_{12}$ sample sintered at 600 °C, the bulk conductivity, σ_b increased from 7.22×10^{-6} S cm^{-1} at 30 °C to 1.38×10^{-5} S cm^{-1} at 500 °C, while for the $LiSn_2P_3O_{12}$ sample sintered at 650 °C, the bulk conductivity, σ_b at 30 °C and 500 °C were 3.28×10^{-6} S cm^{-1} and 1.03×10^{-5} S cm^{-1}, respectively. The highest total conductivity, σ_t was 1.38×10^{-5} Scm^{-1} at 500 °C for the $LiSn_2P_3O_{12}$ sample sintered at 600 °C, which is one order of magnitude above that reported by Norhaniza et al. (2010) and is of the same order of magnitude as reported in our earlier work [18]. By sintering the sample at 600 °C, high density pellet with smaller grains was produced, thus resulting in a higher ionic conductivity value compared to that of the other samples. Furthermore, the $LiSn_2P_3O_{12}$ sample sintered at 600 °C in this work possessed a higher ionic conductivity compared to that of the sample in a previous work by Norhaniza et al. (2010), where traces of impurity still remained. However, the highest total conductivity, σ_t found in the $LiSn_2P_3O_{12}$ sample sintered at 600 °C in this work was slightly lower than that obtained in our previous work, although it was still in the same order of magnitude. The impurity that was present in the samples in our previous work might have contributed to the total electronic conductivity.

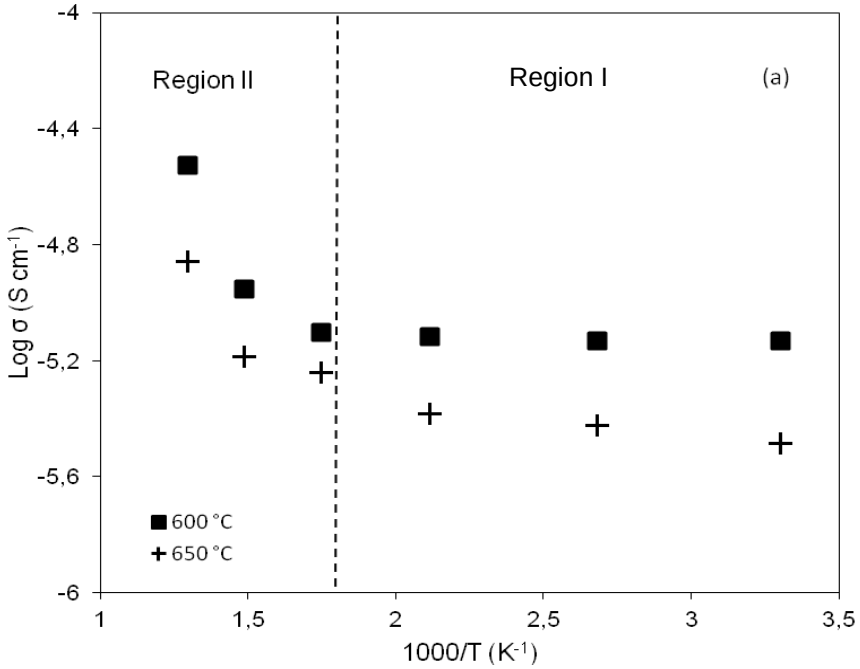

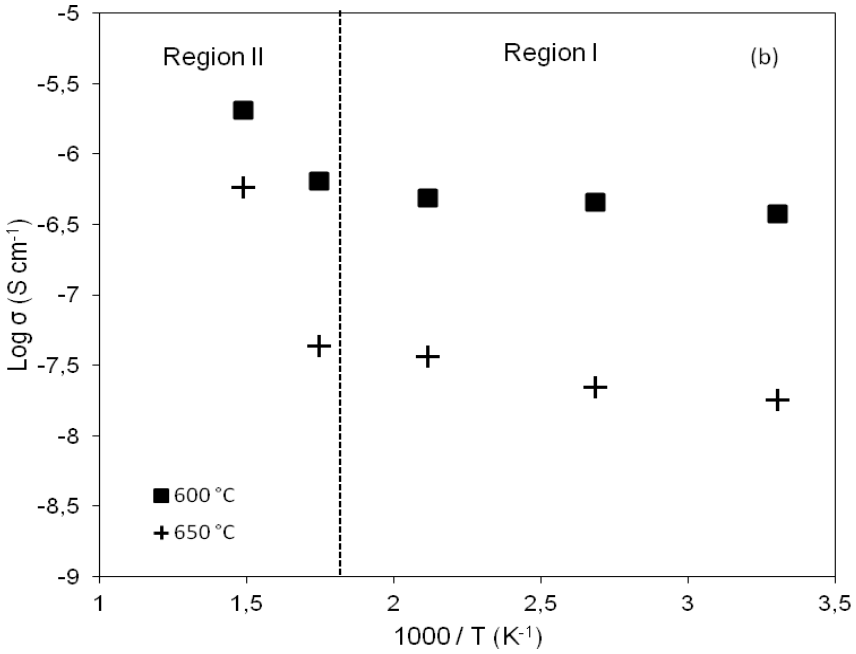

Figure 6. Arrhenius plot showing (a) bulk and (b) grain boundary conductivity of $LiSn_2P_3O_{12}$ samples sintered at 600 and 650 °C.

Figure 6 presents the Arrhenius plot of the (a) bulk and (b) grain boundary conductivity of the $LiSn_2P_3O_{12}$ samples sintered at 600 and 650 °C. The Arrhenius equation below was used to derive the activation energy, E_a for the Li^+ migration:

$$\sigma = \sigma_0 \, exp\left(\frac{-E_a}{kT}\right) \quad (5)$$

where σ is the conductivity, T is the absolute temperature, σ_0 is the pre-exponential factor, E_a is the activation energy for the Li^+ ion migration and k is the Boltzmann's constant. Similar to our previously reported samples [18], two regions can be seen in the Arrhenius plots. The first region, region I can be associated with low temperatures, while region II can be associated with high temperatures. Table 4 gives the values of the bulk and grain boundary activation energies for both regions. The bulk activation energy for the sample sintered at 600 and 650 °C for region I was 0.005 and 0.010 eV, respectively, while the bulk activation energy for the sample sintered at 600 and 650 °C for region II was 0.250 and 0.330 eV, respectively. The same trend applied for the grain boundary activation energy for both samples. Furthermore, the activation energy reported here was much lower than that obtained in other studies as well as in our previous work [8, 11, and 18]. This low activation energy value is typical of a fast ion conductor, and is attributed to the uniform diffusion channels in the NASICON structure [19].

3.6 Electrochemical Stability Window Analysis

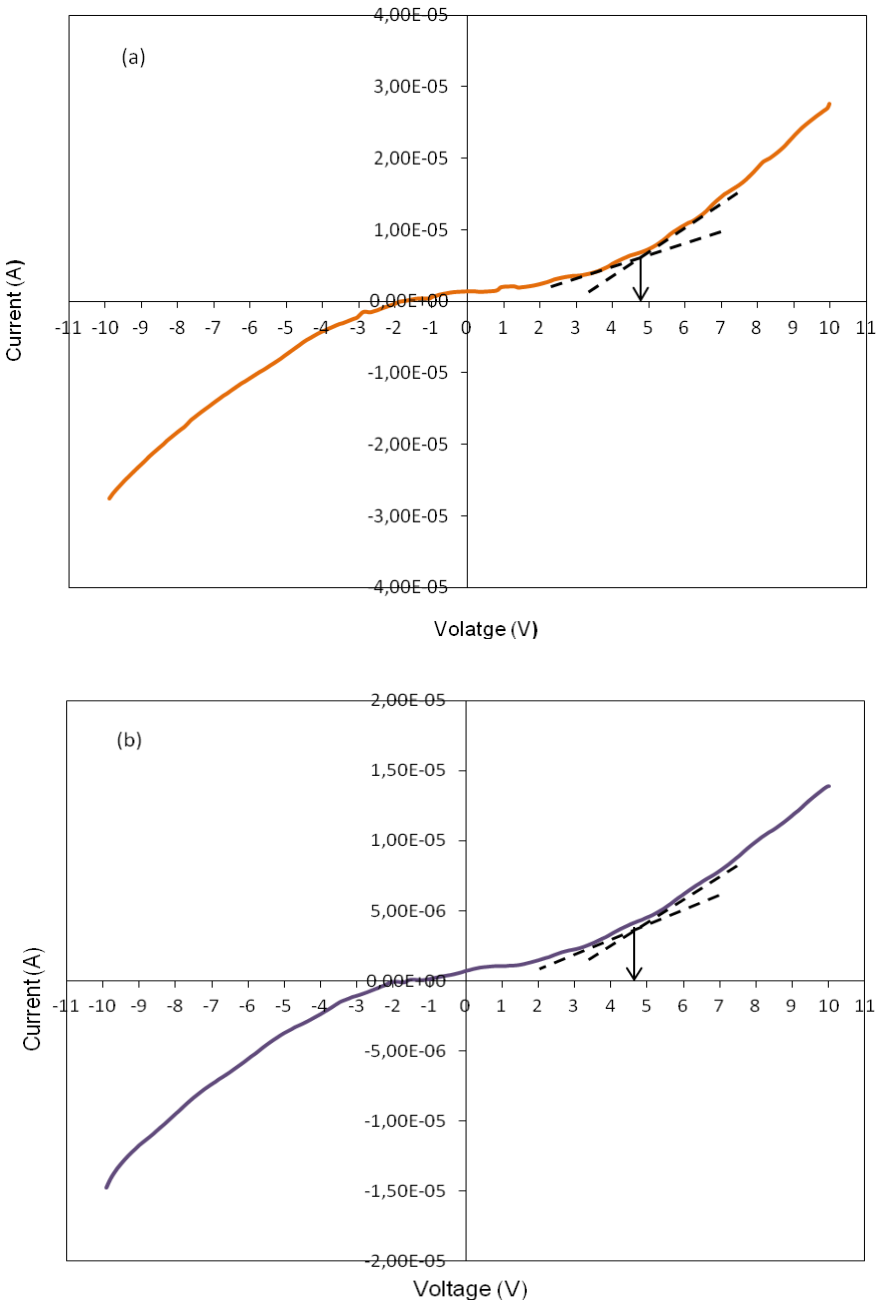

Figure 7. Linear sweep voltammogram of $LiSn_2P_3O_{12}$ samples sintered for 48 hours at (a) 600 and (b) 650 °C

A linear sweep voltammogram was employed in this work to examine the decomposition voltage [24] of the $LiSn_2P_3O_{12}$ electrolyte samples. The linear sweep voltammogram of the $LiSn_2P_3O_{12}$ sample sintered at (a) 600 and (b) 650 °C at room temperature is shown in Figure 7. It can be seen from the figure that the $LiSn_2P_3O_{12}$ sample that was sintered at 600 °C began to decompose at 4.8 V, while the sample that was sintered at 650 °C began to decompose at a lower voltage of 4.6 V. The

value obtained was higher compared to that of the $LiSn_2P_3O_{12}$ samples sintered at 600 °C for 24 hours, which was only 4.4 V [18]. This shows that $LiSn_2P_3O_{12}$ samples with less impurity have a wider electrochemical stability window compared to those samples that contain impurity.

4. CONCLUSIONS

The citric acid assisted sol-gel method was used to successfully synthesize rhombohedral NASICON-structured $LiSn_2P_3O_{12}$ samples with a longer sintering time of 48 hours. The formation of the rhombohedral ($R\bar{3}c$) phase of the $LiSn_2P_3O_{12}$ samples sintered at 600 and 650 °C was verified by XRD and EDX analysis since the longer sintering time resulted in the decomposition of the SnP_2O_7 impurity. The crystallite size produced by the $LiSn_2P_3O_{12}$ samples sintered at 600 °C was smaller than those produced by the samples sintered at 650 °C. At the same time, at 500 ^oC the sample sintered at 600 ^oC had the highest bulk conductivity of 10^{-6} Scm^{-1} at 30 °C and 10^{-5} Scm^{-1} at 500 °C in comparison to the sample sintered at 650 °C. The bulk activation energy was 0.005 eV for the sample with the highest conductivity value for region I (low temperature) and 0.250 eV for region II (high temperature). Besides that, the voltage stability window for both the sintered samples was relatively high at room temperature, reaching 4.8 V and 4.6 V for the samples sintered at 600 °C and 650 °C, respectively. Thus, the current results indicate that $LiSn_2P_3O_{12}$ has a good potential to be employed as a solid electrolyte in electrochemical appliances such as lithium batteries.

ACKNOWLEDGEMENTS
The authors would like to extend their gratitude to the University of Malaya for permitting this research to be carried out. This work was supported by the Fundamental Research Grant Scheme, FP006-2013B by the Ministry of Higher Education, Malaysia and the Postgraduate Research Fund (PPP), PG015-2014A by the University of Malaya. Our highest appreciation goes to Universiti Teknologi Mara (UiTM) and the Ministry of Education, Malaysia for the scholarship under SLAI offered to N. A. Mustaffa.

References

1. L. Vijayan, G. Govindaraj, NASICON Materials: Structure and Electrical Properties, Polycrystalline Materials - Theoretical and Practical Aspects, Prof. Zaharii Zakhariev (Ed.), ISBN: 978-953-307-934-9, InTech, (2012) DOI: 10.5772/28967. Available from: http://www.intechopen.com/books/polycrystalline-materials-theoretical-and-practical-aspects/nasicon-materials-structure-and-electrical-properties.
2. N. Anantharamulu, K. Koteswara Rao, G. Rambabu, B. Vijaya Kumar, V. Radha, M. Vithal, *J. Mater. Sci.*, 46 (2011) 2821.
3. M. Park, X. Zhang, M. Chung, G. B. Less, A. M. Sastry, *J. Power Sources*, 195 (2010) 7904.
4. J. B. Goodenough, H. Y. Hong, J. A. Kafalas, *Mat. Res. Bull.*, 11 (1976) 203.
5. P. P. Kumar, S. Yashonath, *J. Chem. Sci* . , 118 (2006) 135.
6. A. Martinez, J. M. Rojo, J. E. Iglesias, J. Sanz, R. M. Rojas, *Chem. Matter.*, 6 (1994) 1790.
7. A. Martinez-juarez, J. M. Rojo, J. E. Iglesias, J. Sanz, *Chem. Matter.*, 7 (1995) 1857.
8. R. Norhaniza, R, H. Y. Subban, N. S. Mohamed, *Adv. Mater. Res*. , 129 – 131 (2010) 38.

9. W. Cui, J. Yi, L. Chen, C. Wang, Y. Xia, *J. Power Sources* , 217 (2012) 77.
10. J. E. Iglesias, J. Sanz, A. Martinez-Juarez, J. M. Rojo, *J. Solid State Chem.*, 130 (1997) 322.
11. A. Martinez-Juarez, R. Jimenez, P. Duran-Martin, J. Ibanez, J. M. Rojo, *J. Phys. Condensed Matter.*, 9 (1997) 4119.
12. M. G. Lazarraga, J. Ibanez, M. Tabellout, J. M. Rojo, *Compos . Sci . Technol.*, 64 (2004) 759.
13. R. Norhaniza, R. H. Y. Subban, N. S. Mohamed, *J. Matter . Sci .*, 46 (2011) 7815.
14. R. Norhaniza, R. H. Y. Subban, N. S. Mohamed, A. Ahmad, *Int. J. Electrochem . Sci .*, 7 (2012) 10254.
15. R. Norhaniza, R. H. Y. Subban, N. S. Mohamed, *J. Power Sources*, 244 (2013) 300.
16. 16.S. B. R. S. Adnan, N. S. Mohamed, *Ceram . Int.*, 40 (2014) 5033.
17. C. Julien , L. El-Farh, S. Rangan, M. Massot, *J. Sol-Gel Sci. Tec.*, 15 (1999) 63.
18. N. A. Mustaffa, S. B. R. S. Adnan, M. Sulaiman, N. S. Mohamed, *Ionics*, 21 (2015) 955.
19. J. L. Narváez-Semanate, A. C. M. Rodrigues, *Solid State Ionics*, 181 (2010) 1197.
20. C. Mariappan, G. Govindaraj, Solid State Ionics, 176 (2005) 1311.
21. A. Kubanska , L. Castro , L. Tortet , O. Schäf , M. Dollé , R. Bouchet, *Solid State Ionics*, 266 (2014) 44.
22. D. P. Almond, G. K. Dunchan, A. R. West, *Solid State Ionics*, 8 (1983) 159.
23. D. F. Zhou, Y. J. Xia, J. X. Zhu, J. Meng, *Solid State Sciences*, 11 (2009) 1587.
24. P. Georén, G. Lindbergh, *J. Power Sources*, 124 (2003) 213.